Title

High Density Lipoprotein-mediated Cholesterol Uptake and Targeting to Lipid Droplets in Intact L-cell Fibroblasts A SINGLE- AND MULTIPHOTON FLUORESCENCE APPROACH*

Journal

Journal of Biological Chemistry, 275(17)

ISSN

0021-9258

Authors

Frolov, Andrey
Petrescu, Anca
Atshaves, Barbara P
et al.

Publication Date

2000-04-01

DOI

10.1074/jbc.275.17.12769

THE JOURNAL OF BIOLOGICAL CHEMISTRY
Vol. 275, No. 17, Issue of April 28, pp. 12769–12780, 2000

Printed in U.S.A.

High Density Lipoprotein-mediated Cholesterol Uptake and Targeting to Lipid Droplets in Intact L-cell Fibroblasts

A SINGLE- AND MULTIPHOTON FLUORESCENCE APPROACH*

(Received for publication, September 24, 1999, and in revised form, January 13, 2000)

Andrey Frolov‡, Anca Petrescu§, Barbara P. Atshaves§, Peter T. C. So¶, Enrico Gratton‖, Ginette Serrero, and Friedhelm Schroeder§ ‡‡**

*From the ‡Department of Pathobiology, the §Department of Physiology and Pharmacology, Texas A & M University, Texas Veterinary Medical Center, College Station, Texas 77843-4466, the ¶Department of Mechanical Engineering, Massachusetts Institute of Technology, Cambridge, Massachusetts 02139, and the ‖Laboratory for Fluorescence Dynamics, Department of Physics, University of Illinois, Urbana, Illinois 61801, and the **Department of Pharmaceutical Sciences, University of Maryland School of Pharmacy, Baltimore, Maryland 21201-1180*

Fluorescent sterols, dehydroergosterol and NBD-cholesterol, were used to examine high density lipoprotein-mediated cholesterol uptake and intracellular targeting in L-cell fibroblasts. The uptake, but not esterification or targeting to lipid droplets, of these sterols differed >100-fold, suggesting significant differences in uptake pathways. NBD-cholesterol uptake kinetics and lipoprotein specificity reflected high density lipoprotein-mediated sterol uptake via the scavenger receptor B1. Fluorescence energy transfer showed an average intermolecular distance of 26 Å between the two fluorescent sterols in L-cells. Indirect immunofluorescence revealed that both fluorescent sterols localized to L-cell lipid droplets, the surface of which contained adipose differentiation-related protein. This lipid droplet-specific protein specifically bound NBD-cholesterol with high affinity (K_d = 2 nM) at a single site. Thus, NBD-cholesterol and dehydroergosterol were useful fluorescent probes of sterol uptake and intracellular sterol targeting. NBD-cholesterol more selectively probed high density lipoprotein-mediated uptake and rapid intracellular targeting of sterol to lipid droplets. Targeting of sterol to lipid droplets was correlated with the presence of adipose differentiation related protein, a lipid droplet-specific protein shown for the first time to bind unesterified sterol with high affinity.

Because of cholesterol's dual role in both normal cell function and the pathobiology of atherosclerosis, it is essential to resolve the mechanisms whereby exogenous cholesterol is taken up and distributed within the cell (reviewed in Refs. 1–3). Unesterified cholesterol uptake shares some, but not all, aspects of cholesterol ester uptake. Unesterified cholesterol enters the cell either by the slower LDL[1] receptor mediated pathway wherein it leaves the LDL endocytosed within clathrin-coated vesicles prior to vesicle fusion at the lysosome (for review, see Ref. 3) or by the rapid "alternate" HDL receptor pathway (3, 5). However, most attention has focused on the HDL-mediated cholesterol efflux from rather than uptake of cholesterol into the cell (for review, see Ref. 4). Almost nothing is known regarding the uptake and intracellular targeting of unesterified cholesterol via the HDL receptor pathway nor has the process been directly visualized.

Fluorescent cholesterol analogs represent an opportunity for real-time monitoring of the rapid, HDL-mediated uptake of unesterified sterol uptake and movement in living cells. The main requirement for choice of an appropriate fluorescent cholesterol analogue is that it should mimic the behavior of cholesterol. Unfortunately, the functional properties of many fluorescent sterol analogues do not closely resemble those of cholesterol (for review, see Refs. 6–9). The advent of dehydroergosterol (DHE), whose structure closely resembles that of cholesterol, represents a major advance for examining the structure of lipoproteins (10, 11) and membranes (12). DHE is a naturally occurring sterol where it comprises >20% of sterols in certain animals (yeast and sponge) and can replace up to 85% of cultured L-cell fibroblast cholesterol without altering cell growth, membrane function, or membrane lipid composition (for review, see Ref. 6). Furthermore, DHE codistributes with cholesterol in model (2, 6, 13–15) and biological membranes (2, 16–19), desorbs from membranes with very similar kinetics as does cholesterol, and both cholesterol and DHE are esterified in L-cells (2). Finally, DHE readily incorporates into rat, rabbit, or human VLDL, LDL, and HDL either *in vitro* (10, 11, 20, 21) or *in vivo* (21, 22) to reflect the organization of cholesterol and its interactions with apoproteins therein.

Despite the more than two decades wherein DHE was used to determine lipoprotein and membrane structure, only recently were confocal laser scanning microscopy (16) and conventional fluorescence microscopy (23) used to directly visualize intracellular DHE distribution in living cells. It was concluded that DHE colocalized with cholesterol in living cells (23). As both these studies pointed out, however, DHE has very significant disadvantages for use in conventional and confocal microscopy in that DHE requires excitation in the UV region (325

* This work was supported in part by United States Public Health Service, National Institutes of Health Grants GM 31561 (to F. S.), 5P41RR03155 (to E. G.), and DK41463 and American Heart Association Grant 9951222U (to G. S.). These data were presented in part at the 43rd Annual Meeting of the Biophysical Society (Frolov, A., Petrescu, A., Atshaves, B. P., So, P. T. C., Gratton, E., Serrero, G., and Schroeder, F. (1999) *Biophys. J.* **76,** A99, poster 397). The costs of publication of this article were defrayed in part by the payment of page charges. This article must therefore be hereby marked "*advertisement*" in accordance with 18 U.S.C. Section 1734 solely to indicate this fact.

‡‡ To whom correspondence should be addressed. Tel: 409-862-1433; Fax: 409-862-4929; E-mail: fschroeder@cvm.tamu.edu.

[1] The abbreviations used are: LDL, low density lipoprotein; HDL, high density lipoprotein; VLDL, very low density lipoprotein; SR-BI, scavenger receptor BI; DHE, dehydroergosterol; NBD-chol, NBD-cholesterol, 22-(*N*-7-nitrobenz-2-oxa-1,3-diazo-4-yl)-amino-23,24-bisnor-5-cholen-3β-ol)); FRET, fluorescence resonance energy transfer; MLSM, multiphoton laser scanning microscopy; LSCM, laser scanning confocal microscopy; ADRP, adipose differentiation-related protein; FBS, fetal bovine serum; HPLC, high performance liquid chromatography; BSA, bovine serum albumin.

nm) of the spectrum where it becomes severely photobleached.

In the present investigation the disadvantages of UV excitation for DHE were overcome through the use of multiphoton excitation and multiphoton laser scanning microscopy (MLSM). Furthermore, NBD-cholesterol (NBD-chol) proved to be an alternate fluorescent cholesterol analog to visualize HDL-mediated uptake and intracellular targeting of unesterified cholesterol in L-cell fibroblasts. NBD-chol is absorbed by the intestine of hamsters fed NBD-chol as well as by cultured Caco-2 cells (24). In contrast to DHE, the literature with regard to NBD-chol esterification is more complex. NBD-chol is esterified *in vitro* by acyl-CoA cholesterol acyltransferase of hamster intestinal microsomes (24), but not rat liver microsomes (25). Furthermore, NBD-chol is esterified in hamster intestine and cultured Caco-2 intestinal cells (24).

Based on the above findings, the fluorescence properties of DHE and NBD-chol as well as cultured L-cell fibroblasts, a cell line that grows in serum-free medium (26), were used to (i) compare the uptake and esterification of these sterols in the same cell type, (ii) determine if uptake of either fluorescent sterol was characteristic of HDL receptor mediated uptake, (iii) resolve the specificity of intracellular targeting of fluorescent sterol, and (iv) begin to determine the molecular basis for trafficking of cholesterol to lipid droplets.

EXPERIMENTAL PROCEDURES

Materials—DHE was obtained from Sigma or synthesized as described earlier (27). In either case, purity was monitored by HPLC (27) and only DHE with purity >96% was used for the studies presented herein. [^{3}H]Cholesterol was purchased from NEN Life Science Products Inc. (Boston, MA). Human plasma high density lipoproteins (HDL), low density lipoprotein (LDL), and very low density lipoprotein (VLDL) were obtained from Calbiochem, La Jolla, CA. NBD-cholesterol (NBD-Chol), [22-(N-7-nitrobenz-2-oxa-1,3-diazo-4-yl)-amino-23,24-bisnor-5-cholen-3β-ol)], Nile Red, and Alexa 594 goat anti-mouse IgG conjugate were supplied by Molecular Probes (Eugene, OR). Polyclonal and monoclonal anti-caveolin-1 IgM and IgG antibodies were from Transduction Labs (Lexington, KY). Polyclonal anti-scavenger receptor BI (SRB1) antibody was obtained from Novus Biologicals (Littleton, CO). Affinity purified rabbit polyclonal antisera to recombinant mouse adipocyte differentiation-related protein (ADRP) were provided by Dr. G. Serrero (University of Maryland, Baltimore, MD). Alkaline phosphatase and fluorescein isothiocyanate conjugates of goat anti-mouse as well as rabbit IgG and IgM were purchased from Sigma. Texas Red goat anti-rabbit IgG conjugate was from Molecular Probes (Eugene, OR). Nitrocellulose membrane was purchased from Schleicher & Schuell (Keene, NH). All other chemical were reagent grade or better.

Cell Culture and Incorporation of DHE or NBD-chol for Fluorescence Imaging—L-cells (L-arpt$^-$tk$^-$) were maintained in Higuchi medium containing 10% fetal bovine serum as described elsewhere (28). For laser scanning confocal microscopy (LSCM) and MLSM colocalization experiments the L-cells were cultured on Lab-Tek chambered slides (VWR, Sugarland, TX) in Higuchi medium with 10% FBS to which fluorescent sterol was added as indicated. The fluorescent sterols, prepared as ethanolic stock solutions (5–10 mg/ml) containing 1 mol % butylated hydroxytoluene and stored at −70 °C, were then added to the cell culture medium as described earlier (12, 18). The final ethanol concentration was maintained at <0.1%, a level that did not affect cell growth. The choice of fluorescent sterol concentrations for the imaging studies was dictated as follows: (i) because of the low intensity of DHE signal for multiphoton imaging, it was not possible to obtain useable images from cells preincubated with low concentrations (5 μg of DHE/ml of medium). (ii) The use of high levels of NBD-chol (15 μg/ml) in the culture medium cell was prohibitive since it diminished growth and altered cell morphology. Therefore, the L-cells were preincubated in 10% FBS containing medium with or without DHE (15 μg/ml), NBD-chol (5 μg/ml), or (15 μg of DHE +5 μg NBD-chol)/ml, for either 24 or 48 h at 37 °C. After preincubation the L-cells were washed three times with phosphate-buffered saline to remove unbound probe(s) and transferred to Higuchi medium (26) without pH indicator.

Western Blot Analysis of Caveolin 1, SRB-I, and ADRP in L-cells—Cells were lysed in 2% SDS, 10% glycerol in 62.5 mM Tris-HCl, pH 6.8. Protein concentration in cell lysates was estimated by BCA-200 protein assay (Pierce). SDS-polyacrylamide gel electrophoresis was performed on gels containing 40 μg of protein/lane: 16% acrylamide (for caveolin) and 12% acrylamide (for SRB-I and ADRP) (29). Proteins were transferred to nitrocellulose membrane and blots were blocked with: (i) 3% gelatin in TBST (10 mM Tris-HCl, pH 8, 100 mM NaCl, 0.05% Tween 20) when monoclonal anti-caveolin IgM was used; (ii) 0.2% dry milk, 1% gelatin in TBS (TBST without Tween 20) when polyclonal rabbit anti-SRB-I and anti-ADRP were used as primary antibodies. Alkaline-phosphatase conjugates of appropriate secondary antibodies and Western Blue substrate (Promega, Madison, WI) were used to visualize the bands of interest.

NBD-cholesterol Binding to ADRP—Recombinant mouse ADRP used in this experiment was purified according to Serrero *et al.*[2] The affinity of ADRP for NBD-chol was determined using a steady state photon counting fluorimeter (see below) according to a modification of a previously described procedure (30). Briefly, ADRP was added to a 2-ml sample of phosphate buffer (10 mM, pH 7.4) to a final concentration of 11.1 nM. Small increments (0.5–2.0 μl) of NBD-chol (0.14 μM in dimethylformamide) were then added and each sample and blank (without ADRP) were mixed and equilibrated at 25 °C for 2–4 min for stable measurement of fluorescence. NBD-chol was excited at 465 nm (8 nm slits) and fluorescence emission spectra were recorded from 500 to 600 nm (16 nm slits). The NBD-chol fluorescence emission was integrated after each addition of the ligand and corrected for the blank and background. This allowed binding isotherm construction and fitting using a simple, single binding site model as described (30).

Preparation of Cells for Indirect Immunofluorescence Microscopy—L-cells, cultured as described above, were washed with Hank's buffer and fixed in 2% (w/v) paraformaldehyde in Hank's buffer for 30 min at room temperature. In some experiments cells were permeabilized with 0.1% Triton X-100 for 5 min at 4 °C. Cells were then blocked sequentially with 0.2 M glycine for 30 min, and with 0.2 mg/ml goat IgG and 2% bovine serum albumin in Hank's buffer (BSA/Hank's) for 1 h at room temperature. Primary antibodies (monoclonal anti-caveolin-1 IgG and IgM, and rabbit polyclonal anti-SR-BI) were diluted 1:50 in BSA/Hank's and incubated with cells for 2 h at room temperature. Cells were washed three times for 10 min with BSA/Hank's. Secondary antibodies (Alexa, fluorescein isothiocyanate, or Texas Red-labeled goat anti-mouse or rabbit IgG or IgM) were diluted 1:200 in BSA/Hank's and incubated with cells for 1 h at room temperature. Finally, cells were washed and mounted by using the SlowFade kit from Molecular Probes (Eugene, OR). Control experiments included: (i) the lack of specific staining of L-cells with secondary antibody in the absence of primary antibody and (ii) the lack of specific staining of L-cells with preimmune antisera followed by incubation with secondary antibody as described above.

In experiments performed to assess the level of co-localization of ADRP with NBD-chol, L-cells were incubated with 5 μg/ml NBD-chol in Higuchi medium (26) for 48 h prior to fixation in acetone:ethanol mixture (70:30) for 10 min at 4 °C. Cells were then permeabilized with 0.05% saponin for 5 min at room temperature, blocked with 5% FBS in Hank's and incubated with polyclonal rabbit anti-mouse ADRP for 1 h at room temperature. Since NBD-chol has a green fluorescence, Texas Red-conjugated goat anti-rabbit IgG was used to visualize ADRP as red fluorescence; incubation with secondary antibody was for 1 h at room temperature. Cells were then mounted in SlowFade solution as described above.

MLSM and Image Analysis—Multiphoton excitation and MLSM and fluorescence imaging of DHE and NBD-chol was performed on intact L-cells cultured as described above on Lab-Tek chambered slides (VWR, Sugarland, TX). MLSM fluorescence imaging was performed as described elsewhere (31, 32). Briefly, the excitation source was a femtosecond Mira 900 Ti-sapphire laser (Coherent, Palo Alto, CA) pumped at 8 W with an Innova 308 argon ion laser (Coherent, Palo Alto, CA). The Mira 900 Ti-sapphire laser was tuned to emit at 730 or 960 nm, as indicated in the text. The excitation light was delivered to an Axiovert 35 (Zeiss Inc., New York) microscope stage via a modified epiluminescence light path. A Zeiss ×40 Plan-Fluor (1.3 N.A., oil) objective was used for high resolution imaging. The fluorescence signal was collected by the same objective, transmitted through the dichroic mirror and barrier filter (450 SP or 550 LP; CVI Laser, Corp., Albuquerque, NM), and refocused on a low noise, single photon counting R5600-P photomultiplier tube (Hamamatsu, Bridgewater, NJ). Data presentation was performed using MetaMorph Image Analysis Software (Advanced Scientific Imaging, Meraux, LA).

[2] G. Serrero, A. Frolov, F. Schroeder, and L. Gelhaar, submitted for publication.

LSCM and Image Analysis—LSCM studies were performed on a MRC-1024 fluorescence imaging system (Bio-Rad). The system was based on an Axiovert 135 microscope (Zeiss) equipped with three independent low-noise photomultiplier tube channels. The excitation light, λ = 488 nm, from a 15 mW krypton-argon laser (5 mW all lines, measured at the microscope stage) was delivered to the sample through ×63 Zeiss Plan-Fluor oil immersion objective, numerical aperture 1.45. Images were acquired and analyzed using LaserSharp software (Bio-Rad) and MetaMorph Image Analysis Software (Advanced Scientific Imaging, Meraux, LA).

NBD-cholesterol Uptake Kinetics—NBD-chol uptake kinetics were obtained by LSCM fluorescence microscopy on single, living cells. Cells grown to a subconfluent monolayer on chambered coverslips (see above) were washed with Puck's buffer followed by incubation for the indicated time in serum-free, pH indicator-free Higuchi medium without or with the indicated concentration of the following lipid vehicles: FBS, HDL, VLDL, LDL, or BSA. An area on the coverslip chamber containing 5–10 cells was randomly selected with the microscope and the position of the objective was focused to view the median section of the cells. Cholesterol influx was initiated by addition of NBD-chol followed by acquisition of digitally acquiring images at intervals of 30–60 s using TimeCourse Software (Bio-Rad).

Kinetic Analysis of the Time Course of NBD-Chol Uptake—NBD-chol uptake was monitored in single cells as described above and the cell average pixel intensity as a function of time was determined with the help of TimeCourse Software (Bio-Rad). The calculated kinetic parameter values were expressed as mean ± S.E. Statistical analysis was performed using Student's *t* test using the SigmaPlot software (SPSS Inc., Chicago, IL). The kinetics of NBD-chol uptake by L-cells were analyzed by nonlinear regression. The data were best fitted ($r^2 = 0.999$) to the Hill's equation describing cooperative kinetic process,

$$F = (a\ t^b)/(c^b + t^b) \quad \text{(Eq. 1)}$$

where F is the intracellular NBD-chol fluorescence intensity expressed as average pixel intensity in gray scale units; t is the time following the initiation of the influx by addition of NBD-chol; a, b, and c are kinetic parameters describing, respectively, the saturation maximum level, Hill's coefficient, and the time required to reach 50% of the saturation maximum level (t_{50}).

Absorption Spectroscopy—Absorption spectra were recorded on a computer-controlled dual-beam UV-VIS Lambda 2 spectrophotometer (Perkin-Elmer, Norwalk, CT). The background and light scatter correction of the absorption spectra were performed using SigmaPlot software (SPSS Inc., Chicago, IL).

Steady-state Fluorescence Spectroscopy for NBD-chol Binding and Displacement—For NBD-chol binding experiments to ADRP, increasing concentrations of NBD-chol (from 0 to 100 nM) were incubated for 2 min in 25 mM phosphate buffer in the absence or presence of 70 nM ADRP. Emission spectra were then obtained from 500 to 600 nm upon NBD-chol excitation 473 nm. For displacement assays, the ADRP (70 nM) was preincubated with NBD-cholesterol (7 nM) in 25 mM phosphate buffer for 5 min, followed by addition of increasing concentrations of cholesterol (from 0 to 46.5 nM). The spectra were corrected for unbound NBD-cholesterol fluorescence and light scatter. Excitation was at 473 nm while integrative fluorescence intensity was measured for emission >500 nm with a PC1 Photon Counting Spectrofluorometer (ISS Instruments, Champaign, IL) in the ratio mode. Unless otherwise specified, sample temperature was 25 °C (± 0.1 °C) in a thermostatted cell holder. Excitation and emission bandwidths were 4 and 8 nm. Sample absorbance at the excitation wavelengths was < 0.05.

Fluorescence Resonance Energy Transfer (FRET) and the Intermolecular Distance between Dehydroergosterol and NBD-chol—For determination of the average intermolecular distance between DHE and NBD-chol, L-cells were grown under the same conditions used for fluorescence imaging described above: 10% FBS medium with or without DHE (15 μg/ml), NBD-chol (5 μg/ml), or (15 μg of DHE + 5 μg of NBD-chol/ml) for 24 h.

The critical distance for energy transfer, R_0, for the DHE and NBD-chol donor/acceptor pair was calculated a according to Equation 2 (33),

$$R_0 = (9.765 \times 10^3)(K^2 J Q n^{-4})^{1/6} \quad \text{(Eq. 2)}$$

where Q is the quantum yield of the donor in the absence of the acceptor; n, the refractive index; J, the overlap integral defined as,

$$J = \int F_D(\lambda)\varepsilon_A(\lambda)\lambda 4 d\lambda / \int F_D(\lambda) d\lambda \quad \text{(Eq. 3)}$$

where $F_D(\lambda)$ is the normalized emission spectrum of the donor; $\epsilon_A(\lambda)$ is the absorption spectrum of the acceptor. K^2 is the orientation factor ranging from 0 to 4. Giving the n = 1.4, Q = 0.25 (34), and K^2 = 2/3, the critical energy transfer distance for the DHE and NBD-chol donor/acceptor pair was calculated to be 25.8 Å. Energy transfer efficiency, E, is related to the distance between the donor and the acceptor r by,

$$E = R_0^6/(R_0^6 + r^6) \quad \text{(Eq. 4)}$$

HPLC Analysis of Lipids Extracted from Cell Culture—The extent of esterification of [^{3}H]cholesterol, NBD-cholesterol, and DHE was determined by analyzing lipid samples by HPLC. Cell monolayers from L-cells were incubated with either [^{3}H]cholesterol (0.1 μCi/ml medium), NBD-cholesterol (5 μg/ml medium), or DHE (15 μg/ml medium) for 24 h followed by lipid extraction into *n*-hexane/2-propanol (3:2) (v/v) (35). The protein portion was separated by centrifugation (800 × *g*), air-dried, resuspended in 0.2 N KOH, heated overnight at 65 °C, and then quantified for content (36). In order to isolate the neutral lipid classes, the supernatant was evaporated under nitrogen, resuspended in chloroform/methanol (59:1), and applied to a silicic acid column. The eluate was evaporated to dryness, brought up in hexane (98.7), isopropyl alcohol (1.2), glacial acetic acid (0.5), hexane (75:25) (v/v), and injected onto a Luna 5-μm Silica (2) column (Phenomenex, Torrance, CA). Data was analyzed by software from Dionysis Peak net (37, 38).

RESULTS

Uptake and Intracellular Esterification of Dehydroergosterol and NBD-chol in L-cell Fibroblasts—Two fluorescent sterols, DHE and NBD-chol, were used herein to directly visualize sterol uptake as well as intracellular sterol distribution and targeting. DHE is a naturally occurring fluorescent sterol while NBD-chol is a synthetic sterol containing the NBD reporter group attached in the alkyl chain of cholesterol. Because of the use of different *in vitro* and *in vivo* conditions in the literature (see Introduction), it is difficult to compare their relative uptake and/or esterification. Therefore, DHE and NBD-chol uptake and intracellular esterification were compared in the same cell line, L-cell fibroblasts, and under the same conditions used for the fluorescence imaging and fluorescence resonance energy transfer studies described in the following sections.

The extent of DHE and NBD-chol taken up by L-cells differed markedly. When cultured in 10% FBS serum supplemented with 5 or 15 μg of DHE/ml medium, respectively, L-cells took up 13.5 ± 1.2 (n = 5) and 73.5 ± 13.2 (n = 4) pmol of DHE/mg of cell protein, respectively. While morphological and cell growth changes precluded determination at high NBD-chol (15 μg of NBD-chol/ml medium), L-cells grew normally at 5 μg of NBD-chol/ml medium and took up 0.16 ± 0.01 pmol of NBD-chol/mg cell protein (n = 5). Thus, total uptake of DHE was 84- and >100-fold, respectively, greater than that of NBD-chol.

Comparison of the half-times of DHE and NBD-chol uptake also revealed significant differences. The half-time of DHE uptake by L-cells is about 1 day (12), similar to that for [^{3}H]cholesterol (39). In contrast, the half-time of NBD-chol uptake was much faster, 6 min (see below). Therefore, the half-time of DHE uptake was >100-fold slower than that of NBD-chol.

Finally, the intracellular esterification of DHE and NBD-chol by L-cell fibroblasts differed much less than observed for uptake and half-time of uptake. HPLC of lipid extracts from L-cells supplemented with DHE showed two peaks, near 3 min (DHE-ester) and 19 min (DHE), respectively (Fig. 1*A*). When the cells were cultured with 5 and 15 μg of DHE/ml medium, 5.2 ± 0.5% (n = 5) (not shown) and 27.6 ± 9.0% (n = 4) (Fig. 1*C*) of the DHE taken up was esterified, respectively. This was 1.4-fold (not shown) and 7.5-fold (Fig. 1*C*), respectively, more than that of [^{3}H]cholesterol (Fig. 1*C*). The same HPLC system also resolved lipid extracts from NBD-chol (5 μg of NBD-chol/ml of medium) supplemented L-cells into two peaks with retention times near 5 min (NBD-chol ester) and 17 min (NBD-chol) (Fig. 1*B*). The NBD-chol ester represented only 7.8 ± 0.4% (n = 5) of total NBD-chol taken up (Fig. 2*C*), only 2-fold more

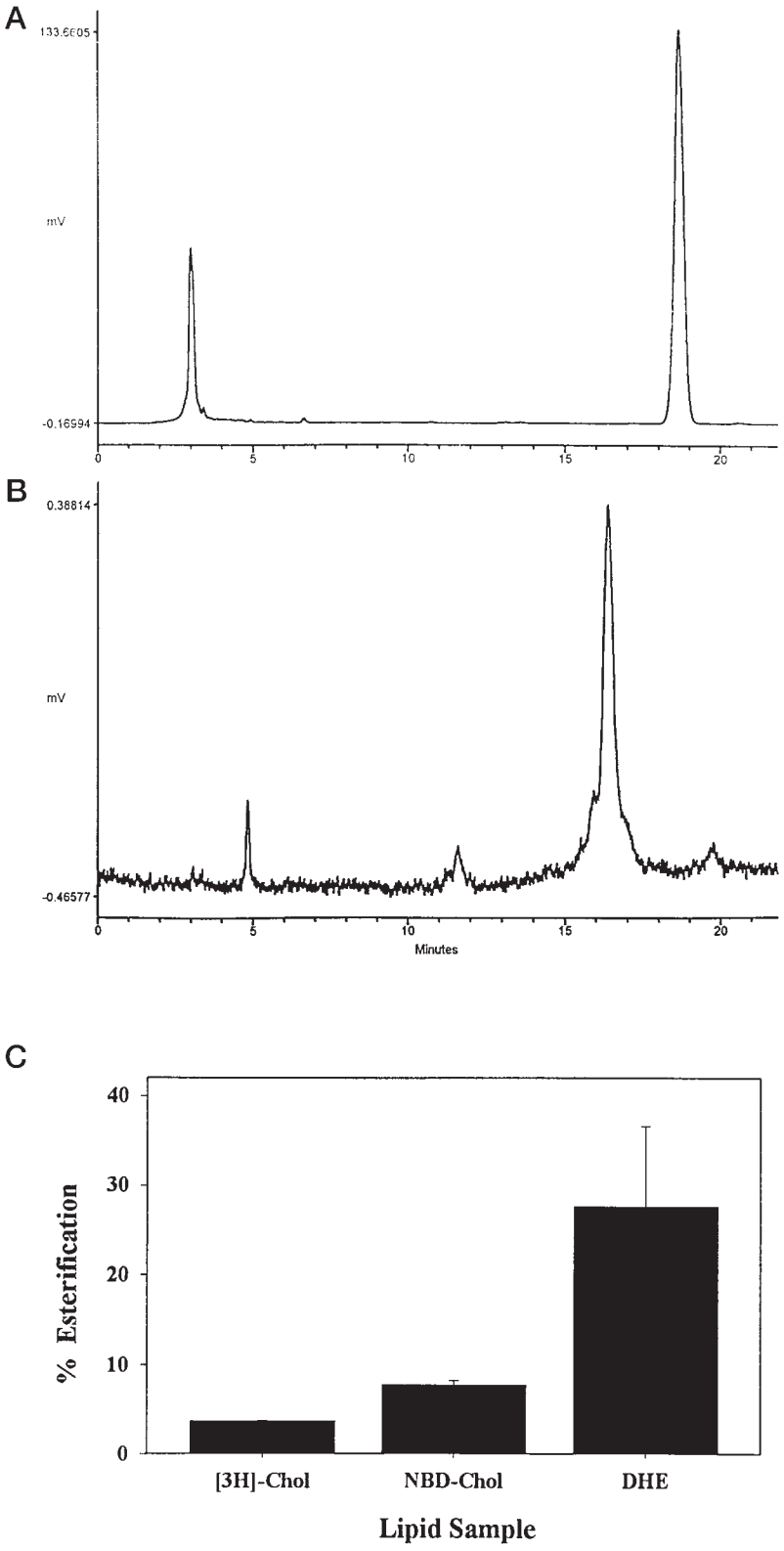

FIG. 1. **Intracellular esterification of sterols in cultured L-cell fibroblasts.** DHE, NBD-cholesterol, and [^{3}H]cholesterol were individually incorporated into L-cells as described under "Experimental Procedures." Lipids were extracted from L-cells after 24 h incubation in complete medium as described under "Experimental Procedures." *Panel A,* high performance liquid chromatogram of DHE detected by absorbance at 324 nm. *Panel B,* high performance liquid chromatogram of NBD-chol detected by absorbance at 443 nm. *Panel C,* extent of esterification of [^{3}H]cholesterol, NBD-cholesterol, and DHE after 24 h incubation. Values represent mean ± S.E. from four to five experiments.

than that of [^{3}H]cholesterol (Fig. 1*C*). Thus, under the conditions necessary for obtaining optimal fluorescence images and energy transfer (see below), DHE was esterified 3.5-fold more than NBD-chol.

In summary, both DHE and NBD-chol were taken up by L-cell fibroblasts and esterified intracellularly. In contrast to the 2 order of magnitude differences in uptake parameters, however, the two fluorescent sterols differed much less in proportion esterified, especially when cultured in the presence of equimolar DHE or NBD-chol (5.2% *versus* 7.8% esterified). This suggested that while DHE and NBD-chol uptake may differ, once internalized both sterols appeared to share a similar intracellular esterification pathway and, as shown below, similar intracellular targeting.

The Intracellular Distribution of DHE in L-cell Fibroblasts: Multiphoton Laser Scanning Microscopy—As indicated in the Introduction, the UV excitation (maximum near 320 nm) required for DHE excitation resulted in high photobleaching of

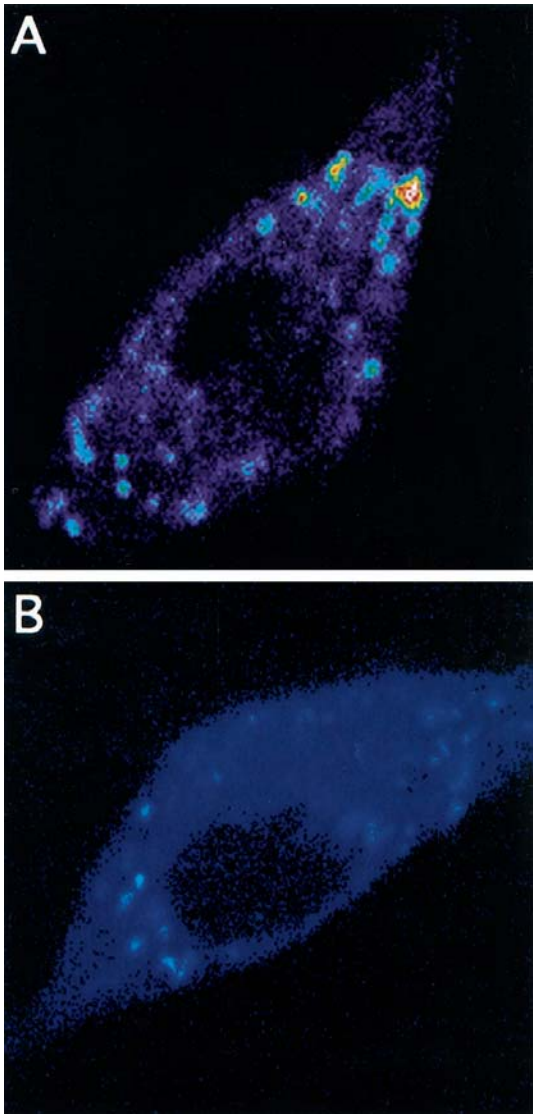

FIG. 2. **Multiphoton excitation fluorescence imaging of DHE and NBD-cholesterol in intact L-cell fibroblasts.** *A,* three-photon excitation DHE fluorescence in L-cells. Cells were preincubated with 12 μg/ml DHE for 24 h in serum containing medium as described under "Experimental Procedures." Excitation wavelength 930 nm. *B,* two-photon excitation NBD-cholesterol fluorescence in a separate set of L-cells. Cells were preincubated with 5 μg/ml NBD-cholesterol for 24 h in serum containing medium. Following incubation with fluorescent probes, cells were washed three times with phosphate-buffered saline to remove unbound probe and transferred into the Puck's buffer, pH 7.4. The images were obtained at room temperature. For more details see "Experimental Procedures."

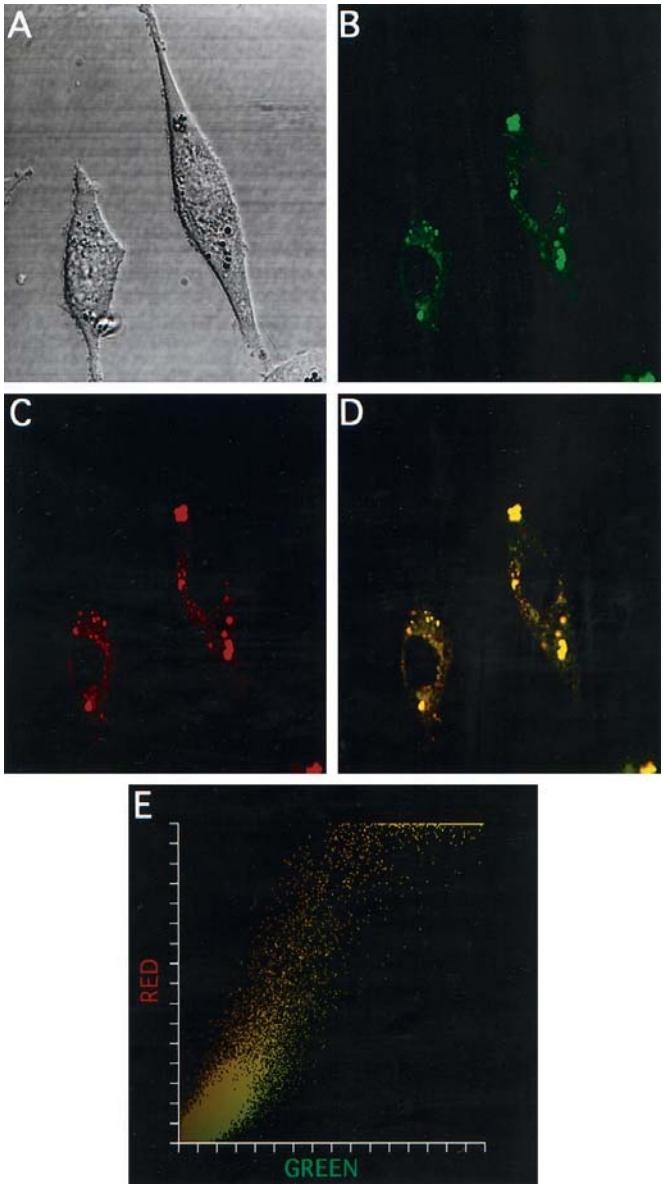

FIG. 3. **Intracellular localization of NBD-cholesterol in L-cells dually labeled with NBD-cholesterol and Nile Red.** *A,* transmitted light image obtained with a Bio-Rad MRC-1024 laser scanning fluorescence microscope using the transmitted light detector mode. The transmitted light image showed the outline and overall morphology of the cell. Visible are the highly refractile lipid droplets. *B,* single-photon excitation LSCM Image of NBD-cholesterol. *C,* single-photon excitation LSCM Image of Nile Red. *D,* sequentially acquired images B and C were superimposed to yield a merged image. Colocalized NBD-chol and Nile Red appeared as *yellow-orange* punctate structures. *E,* pixel fluorogram of the merged image showing the high degree of NBD-chol and Nile Red fluorescence spatial correlation in L-cells. NBD-cholesterol was excited with the 488-nm laser line and fluorescence emission detected with a 530/20 band pass filter. Nile Red was excited with 568 nm laser line and emission detected with a 680/30 band pass filter. For more details see "Experimental Procedures."

DHE. This drawback coupled with potential phototoxicity of exposing living cells containing DHE to high energy UV radiation for extended periods of time, seriously complicated the use of LSCM or conventional fluorescence microscopy for visualizing the intracellular distribution of DHE. Fortunately, these drawbacks of UV excitation can be circumvented by multiphoton infrared excitation and MLSM (40, 41).

Although two-photon excitation and MLSM of DHE in L-cells allowed detection of DHE, this was complicated by simultaneous autofluorescence. At the lower wavelength limit of the Ti/Sa laser (about 680–700 nm) two-photon excitation of DHE simultaneously excited endogenous NADH resulting in high autofluorescence in the L-cells (data not shown).

In contrast, three-photon excitation conditions allowed selection of excitation wavelength at which no detectable autofluorescence was observed by MLSM. DHE excitation equivalent to about 310 nm was achieved by combining the energy of three infrared photons with 930 nm wavelength. Under three-photon conditions these photons were simultaneously absorbed by the DHE chromophore which subsequently displayed stable emission. Three-photon MLSM of DHE in L-cells detected DHE inside the cells, highly localized in large punctate areas with additional diffuse emission (Fig. 2*A*). This pattern of DHE distribution to large punctate areas resembled that of lipid droplets visible by transmission microscopy (Fig. 3*A*).

Multiphoton Laser Scanning Microscopy of NBD-cholesterol

in L-cell Fibroblasts—It is not known whether NBD-chol (a synthetic sterol with NBD group attached in the acyl chain of cholesterol) exhibits a similar intracellular distribution as DHE, a naturally occurring sterol that codistributes with cholesterol (see Introduction) in L-cells. To examine the intracellular distribution of NBD-chol, the fluorescent sterol was incorporated into L-cells exactly as described for DHE except that two-photon excitation at 930 nm was used. The simultaneous absorption of two-photons at 930 nm was equivalent to single photon excitation at 465 nm, a wavelength at which NBD-chol efficiently absorbs while autofluorescence was negligible (not shown). MLSM of NBD-chol in L-cells displayed a very similar punctate intracellular fluorescence pattern (Fig. 2*B*) as was observed by MLSM of DHE (Fig. 2*A*) in L-cells. The pattern of NBD-chol distribution (Fig. 2*B*) also resembled that of lipid droplets visible by transmission microscopy (Fig. 3*A*).

Colocalization of NBD-cholesterol to Lipid Droplets in Intact L-cell Fibroblasts by LSCM—In order to determine if the fluorescent sterol probes were present in lipid droplets, colocalization experiments were performed with Nile Red, a neutral lipid specific probe known to stain lipid droplets (42, 43). Unfortunately, because of the photophysics of three-photon excitation, the low quantum yield of DHE, and the instrumental limitations, the emission of DHE was too weak for simultaneous colocalization with Nile Red.

In contrast to DHE, the spectral properties of NBD-chol were ideal for single-photon excitation and imaging by LSCM in order to establish whether the punctate distribution of NBD-chol observed above was due to its presence in lipid droplets. Therefore, L-cells were dually labeled with NBD-chol and Nile Red as described under "Experimental Procedures" and imaged by LSCM (Fig. 3). The red colored intracellular punctate structures obtained with Nile Red (Fig. 3*C*) were clearly visible on the transmitted light image (Fig. 3*A*) and appeared almost identical with the intracellular distribution pattern of the green punctate structures detected by NBD-cholesterol acquired simultaneously in L-cells (Fig. 3*B*). Colocalization of the Nile Red and NBD-chol would be visualized as a merging of red and green to yield a orange-yellow punctate distribution. Indeed, a merged image of Nile Red and NBD-chol (Fig. 3*D*) revealed a distinctly orange-yellow punctate distribution. The respective fluorogram (Fig. 3*E*) constructed from the merged image further confirmed the high degree of the fluorescence spatial colocalization of these probes. The size of the lipid droplets revealed by colocalization of NBD-chol (Fig. 3*B*) and Nile Red (Fig. 3*C*) as well as by transmission microscopy (Fig. 3*A*) ranged from 0.3–0.5 μm. In summary, NBD-chol was taken up by L-cells and targeted to lipid droplets.

Proximity of DHE and NBD-cholesterol in Dual-labeled L-cell Fibroblasts as Probed by FRET—Although NBD-chol was highly colocalized within large punctate structures identified as lipid droplets (Nile Red) and DHE also distributed to similar punctate structures in L-cells, the spatial resolution of light microscopy is only 0.3 μm. To achieve Å level resolution necessary to determine the intermolecular distance between NBD-chol and DHE within the lipidic structures, it was necessary to use FRET. The fluorescence emission spectrum of the donor (DHE) overlapped significantly with the absorption spectrum of the acceptor (NBD-chol) (not shown), a primary criterion necessary for efficient FRET (33).

The FRET from DHE to NBD-chol in L-cells was examined by MLSM. L-cells were dual labeled with (15 μg of DHE + 5 μg of NBD-chol)/ml medium and excited at 930 nm. Under these conditions (simultaneous three-photon excitation of DHE and two-photon excitation of NBD-chol) the level of the DHE emission (but not NBD-chol) in lipid droplet structures of L-cells was qualitatively lower (data not shown). Unfortunately, the low intensity of the DHE emission in these images did not allow accurate determination of R, the intermolecular distance between DHE and NBD-chol.

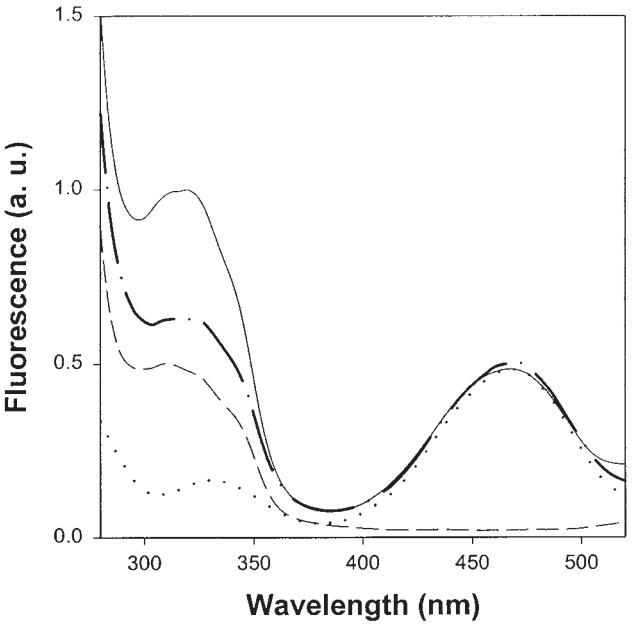

FIG. 4. **Fluorescence energy transfer between DHE and NBD-cholesterol in L-cell fibroblasts.** Representative spectra (viewed from *top* to *bottom* at 325 nm) were as follows. *Solid line* was the fluorescence excitation spectrum of the cells dually labeled with DHE (15 μg/ml) and NBD-cholesterol (5 μg/ml) in serum containing medium as described under "Experimental Procedures." *Dash-dot line* was the combined fluorescence excitation spectra of the single fluorescent sterol (DHE or NBD-chol) labeled cells. *Dashed line* was the fluorescence excitation spectrum of L-cells labeled with 5 μg/ml DHE. *Dotted line* was the fluorescence excitation spectrum of L-cells labeled with NBD-cholesterol (5 μg/ml). Combined spectra were obtained as follows. The DHE and NBD-cholesterol fluorescence excitation spectra in the single-labeled cells were corrected according to the DHE and NBD-cholesterol concentration in the dual-labeled cells, added together, and normalized to the intensity at 460 nm. Fluorescence was detected at 550 nm. For more details, see "Experimental Procedures" and the text. At the end of the incubation cycle, cells were washed three times with phosphate-buffered saline to remove the unbound probe, trypsinized, and centrifuged. Following centrifugation, cells were resuspended in the Puck's buffer, counted, diluted to 2×10^5 cells/ml, and transferred into a photon counting spectrofluorimeter or spectrophotometer for the spectral analysis as described under "Experimental Procedures."

To obtain quantitative data for determining R, FRET between DHE and NBD-chol was determined with L-cells in suspension by use of a very sensitive photon counting fluorometer. Again, L-cells were cultured in 10% FBS medium with or without DHE, NBD-chol as described above. Following incubation, the cells were washed and fluorescence excitation spectra were obtained as described in the legend of Fig. 4. The excitation spectrum (detected at the NBD-cholesterol emission maximum, λ_{em} = 550 nm) of L-cells labeled only with NBD-chol (Fig. 4) revealed a small excitation maximum near 330 nm and a major excitation maximum at 460 nm. In contrast, the excitation spectrum (detected at the NBD-cholesterol emission maximum, λ_{em} = 550 nm) of L-cells labeled only with DHE exhibited only an excitation maximum near 325 nm and no excitation maximum near 460 nm (Fig. 4). However, the excitation spectrum of the dual-labeled cells (detected at the NBD-cholesterol emission maximum, λ_{em} = 550 nm) displayed a strong excitation maximum at ~325 nm and a 2-fold weaker excitation maximum at ~460 nm. Under the same experimental conditions, the non-labeled cells exhibited no detectable fluorescence signal. The data obtained indicated that in the

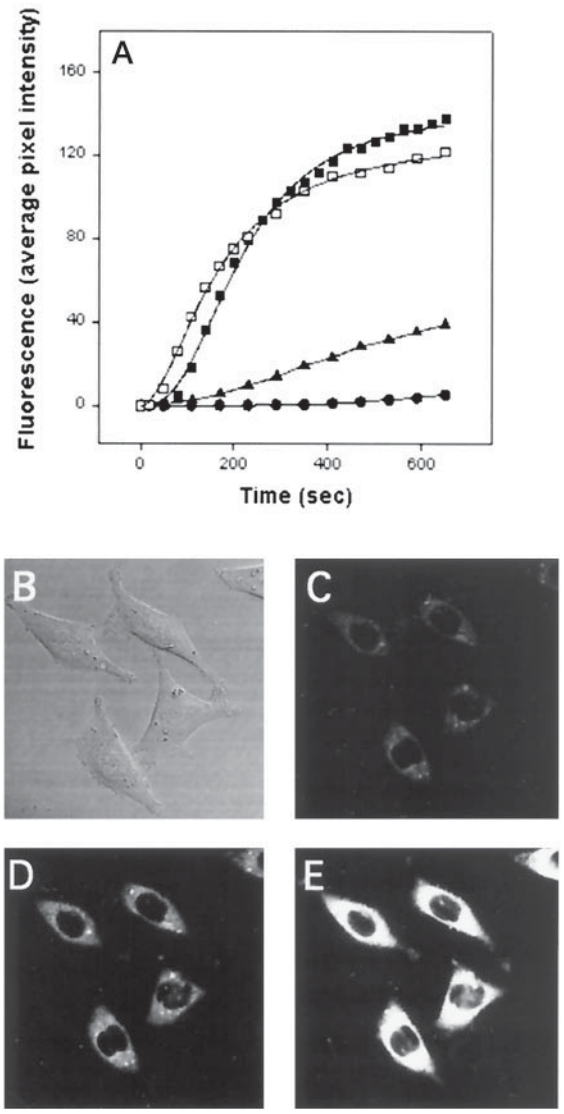

FIG. 5. **Kinetics of unesterified cholesterol influx in L-cell fibroblasts in the presence of lipid vehicles.** *A,* NBD-chol uptake kinetics shown as average fluorescence pixel intensity per cell. *Closed squares,* medium containing 5% fetal bovine serum; *open squares*, serum-free medium + 17 μg/ml HDL; *closed triangles,* serum-free medium + 50 μM BSA; *closed circles,* serum-free medium. The half-time of NBD-chol uptake in serum-free medium alone could not be accurately measured. However, extrapolation of the baseline suggested a half-time >85 min. *B,* transmitted light image of L-cells monolayer; *C-E*, single-photon excitation LSCM images of NBD-cholesterol fluorescence in L-cells (5% fetal bovine serum) 30, 60, and 120 s after addition of 0.5 μg/ml NBD-cholesterol. The bright staining intracellular structures were lipid droplets. The digitized fluorescence signal was corrected for the background measured outside the cells. The background fluorescence was <0.5% of the maximal NBD-cholesterol signal in all cases studied. At least three independent series of experiments were performed and representative curves are shown. For more details, see "Experimental Procedures."

dual-labeled cells, NBD-cholesterol solely contributed to the observed excitation maximum at ~460 nm, while the excitation fluorescence band at ~325 nm was predominantly due to DHE.

If FRET occurred from DHE to NBD-cholesterol in the dual-labeled cells, the DHE excitation band intensity at ~325 nm (while detecting predominantly NBD-cholesterol emission at 550 nm) was expected to increase. This possibility was examined as follows. (i) The DHE and NBD-cholesterol excitation fluorescence spectra acquired separately in the single-labeled cells were corrected for the difference in DHE and NBD-cholesterol concentration in the dual-labeled cells (Fig. 4, *bottom two curves*). (ii) The intracellular probe concentration was measured in the same samples by the means of absorption spectroscopy. (iii) The corrected single DHE and NBD-cholesterol spectra were added together and normalized to the intensity of NBD-cholesterol band at ~460 nm (Fig. 4, *second curve* from the *top*). This allowed construction of the mathematically combined curve obtained under conditions of no energy transfer, *i.e.* from cells labeled separately with NBD-chol or DHE, but not both (Fig. 4, *second curve* from the *top*). Comparison to the curve for dual-labeled cells (both DHE and NBD-chol) also normalized to the intensity at ~460 nm (Fig. 4, *top curve*), clearly demonstrated that the intensity of the NBD-cholesterol excitation at ~325 nm was indeed increased in the dual-labeled cells as compared with a mathematical combination from cells loaded separately with DHE or NBD-cholesterol. This allowed calculation of the critical energy transfer distance R_0 = 25.8 Å. From these data and using a R_0 = 25.8 Å (see "Experimental Procedures"), the average distance R between DHE and NBD-chol in the dual-labeled cells (Equation 3) was estimated to be 26 Å.

It must be considered that the average distance R between DHE and NBD-chol, 26 Å, may reflect contributions from both the unesterified and esterified fluorescent sterols. This possibility was based on the fact that 27.6% and 8% of DHE and NBD-chol were esterified, respectively (Fig. 1), under the conditions used for FRET. The relative contributions of the esterified fluorescent sterols may be evaluated based on the structure of lipid droplets which is basically a nonpolar lipid core (sterol esters and triacylglycerols) surrounded by a more polar surface polar monolayer (sterols and phospholipids) (44, 45). The nonpolar core of L-cell lipid droplets is cholesterol ester-rich (cholesterol ester/triacylglycerol ratio of 30:1) (46), typical of lipid droplets in tissues such as adrenal (cholesterol ester/triacylglycerol ratio of 8:1) (44). This suggests three possible types of FRET. (i) From DHE donor to NBD-chol acceptor in the lipid droplet polar monolayer. Since the majority (93%) of NBD-chol was not esterified and unesterified sterols readily phase separate into sterol-rich domains (2), conditions were favorable for FRET between DHE and NBD-chol in the lipid droplet monolayer. (ii) From DHE-ester donor to NBD-chol ester acceptor in the lipid droplet nonpolar core. The orientation factor between these sterol esters in the core was not as favorable as that in the surface monolayer due to the more random orientation as well as higher fluidity of the neutral lipid core (10, 11). These factors, along with the several order of magnitude greater volume of dilution of the lipid core, did not favor FRET. (iii) From DHE donor in the lipid droplet surface monolayer and NBD-chol ester acceptor in the core of the lipid droplet. The diameter of the L-cell lipid droplets was 3000–5000 Å, while the thickness of a polar lipid monolayer was much smaller, 25 Å. Because of this 120–200-fold greater thickness of the neutral lipid core, the majority of NBD-chol ester acceptor was not likely near the DHE donor in the surface monolayer. The higher fluidity of the neutral lipid core also yielded a less favorable orientation factor for energy transfer. These considerations, taken together with energy transfer varying as R^{-6}, resulted in much lower efficiency of energy transfer from the surface monolayer to the core than within the surface monolayer (10, 11).

In summary, FRET revealed the average intermolecular distance between DHE and NBD-chol to be 26 Å, >100-fold closer than that resolvable by optical microscopy. The 26-Å intermolecular distance was easily encompassed within the lipid droplets whose diameter (range from 0.3 to 0.5 μm, see above) was 120–200-fold greater. Finally, the cross-sectional diameter of cholesterol, about 13 Å, suggests that on average the DHE and NBD-chol were separated by no more than the thickness of another lipid molecule, regardless of whether these fluorescent

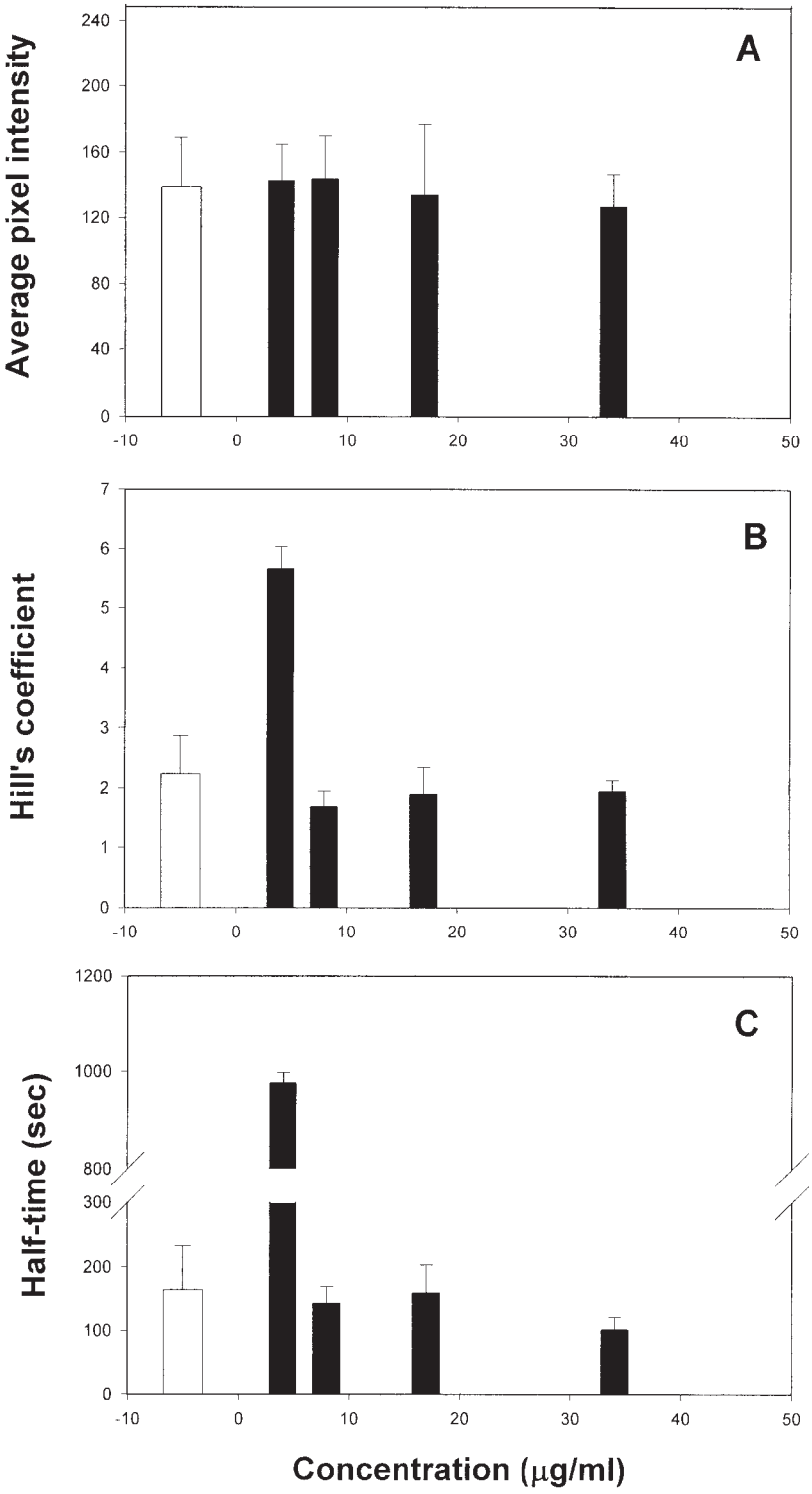

FIG. 6. **Kinetic parameters of NBD-cholesterol influx in L-cell fibroblasts.** All parameters of NBD-chol uptake were measured in serum-free medium supplemented with the indicated concentration of HDL. The maximal fluorescence intensity (*A*), the Hill coefficient (*B*), and the half-time parameters (*C*) were obtained from the respective kinetics as described under "Results." NBD-cholesterol concentration was 0.5 μg/ml. *Abscissa,* HDL concentration, μg/ml. All experiments were performed at 25 °C. Data are mean ± S.E. (n = 14–79).

sterols were esterified or whether they were located in the lipid droplet surface or interior core.

Uptake kinetics of NBD-cholesterol into L-cell Fibroblasts: a LSCM Investigation—NBD-chol allows direct visualization of the uptake of unesterified sterol into living cells. In the absence of serum the uptake of NBD-chol into the L-cells was very slow, as shown by the cellular fluorescence near baseline and half-time to reach maximum cellular fluorescence >85 min (Fig. 5*A, solid circles*). Serum markedly enhanced NBD-chol uptake ($t_{½}$ = 6.1 ± 0.8 min, maximum near 10 min). In the presence of serum, NBD-chol uptake exhibited sigmoidal kinetics (Fig. 5*A, solid squares*) as well concentration dependence up to 0.5 μg/ml and approached saturation (Fig. 5*A*). However, saturation was still not complete even at the highest NBD-chol concentration (3 μg/ml). The Hill coefficient (b ~ 2.6) of serum mediated NBD-chol uptake was independent of NBD-chol concentration (data not shown), consistent with a multicomponent uptake. In contrast, the half-time of NBD-chol uptake into L-cells decreased by almost 5-fold, from 6.1 ± 0.8 min to minimum near 1.3 ± 0.6 min, over a 15-fold increase in NBD-cholesterol concentration in the medium (data not shown).

Uptake Kinetics of NBD-cholesterol into Specific Intracellu-

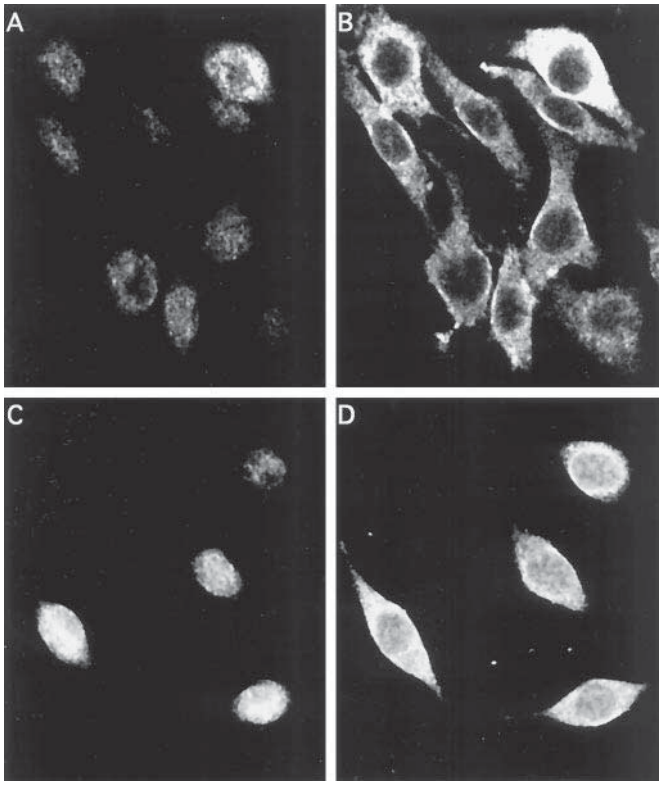

FIG. 7. **Indirect immunofluorescence of caveolin-1 (*A* and *B*) and scavenger receptor type B-I (*C* and *D*) in L-cells.** Optical sections were taken from Z-scan single-photon excitation LSCM images at 6 μm (*A* and *C*) and 9 μm (*B* and *D*) from the bottom of the chambered slide. The fluorescence emission of the caveolin-1 and SRB-I secondary antibodies labeled with Alexa 594 was obtained after excitation with 568 nm laser line and emission selected with a combination of 640LP and 680/30 band pass filters.

lar sites in L-cell Fibroblasts: Targeting to Lipid Droplets as Determined by LSCM—In the absence of serum, NBD-chol uptake into lipid droplets was essentially not detectable over the 10-min time period examined (not shown). In contrast, in the presence of serum NBD-chol was detected in lipid droplets within 30 s (Fig. 5*C*), followed by its gradual increase in the cytoplasmic area (60 and 120 s, Fig. 5, *D* and *E*). Uptake of NBD-chol into lipid droplets was very fast ($t_{½}$ = 5.8 ± 0.7 min) and essentially the same as that observed into the whole cell ($t_{½}$ = 6.1 ± 0.8 min). Thus, NBD-chol was extremely rapidly, <30 s, transferred from the cell surface to lipid droplets in L-cells.

Specific Components of Serum Mediating Rapid Uptake of Unesterified Cholesterol in L-cell Fibroblasts as Determined by NBD-chol—Albumin only weakly stimulated NBD-chol uptake as compared with serum with onset near 3 min (>3-fold longer than with serum), and extrapolated time to achieve maximum uptake of hours (Fig. 5*A, solid triangles*). In contrast, HDL (17 μg/ml) dramatically stimulated NBD-chol uptake with onset <30 s (Fig. 5*A, open squares*) and $t_{½}$ = 2.6 ± 0.7 min which was 60% shorter than of serum, $t_{½}$ = 6.1 ± 0.8 min (Fig. 5*A, open versus closed squares*). In contrast, the other serum lipoproteins (17 μg/ml) were less effective: LDL, $t_{½}$ = 5–7 min; VLDL, $t_{½}$ = 11 min. Furthermore, while HDL and LDL mediated NBD-chol uptake fit the Hill's equation, VLDL mediated NBD-chol uptake did not. However, in all cases intracellular targeting of NBD-chol was to lipid droplets. In summary, NBD-chol detected the existence of a fast, lipoprotein-dependent (HDL > LDL > VLDL) mechanism(s) for uptake and targeting of unesterified sterol to lipid droplets. Since LDL and VLDL interact within endocytic uptake (LDL receptor, VLDL receptor) as well as non-endocytic uptake (HDL receptors), but do not effectively compete with HDL for binding to the HDL receptor (reviewed in Ref. 4), NBD-chol uptake was the average of both processes. Since HDL does not bind to the LDL receptor, this allows select examination of the uptake kinetics of unesterified cholesterol via the HDL receptor pathway alone.

Concentration Dependence and Kinetic Analysis of HDL-mediated NBD-chol Uptake in L-cell Fibroblasts—The HDL-dose dependence of the unesterified sterol uptake was studied at an NBD-chol (0.5 μg/ml) concentration far from saturating intracellular NBD-cholesterol fluorescence. The maximal fluorescence of NBD-chol uptake in L-cells was independent of HDL concentration from 0 to 34 μg/ml (Fig. 6*A*), essentially the same as that in serum-containing medium (Fig. 5*A*). The Hill coefficient of NBD-chol uptake decreased 3-fold between 4 and 34 μg of HDL/ml (Fig. 6*B*) to resemble than in serum containing medium. The $t_{½}$ of NBD-chol uptake decreased 42-fold from 0 to 34 μg of HDL/ml (Fig. 6*C*), >3-fold faster than that in serum-containing medium. Interestingly, at higher concentrations of LDL or VLDL these lipoproteins had the opposite effect on $t_{½}$ of NBD-chol uptake and actually increased the half-time of NBD-chol uptake 2–3-fold (data not shown). Thus, increasing LDL or VLDL (but not HDL) slowed NBD-chol uptake, reflecting increasing contributions of the slower endocytic processes mediated via LDL and VLDL receptors. When the medium HDL concentration was held constant (17 μg/ml) and the NBD-chol concentration was increased from 0.2 to 1 μg/ml the half-time of HDL-mediated NBD-chol uptake significantly decreased almost 5-fold, from 7.3 ± 1.2 min to 1.3 ± 0.4 min (n = 14–79). Thus, at higher concentrations the HDL enhanced more rapid HDL receptor mediated uptake of unesterified sterol while higher LDL or VLDL concentrations enhanced the slower endocytic uptake of unesterified cholesterol.

Examining the Molecular Basis of HDL-mediated Unesterified Cholesterol Uptake in L-cells—HDL-mediated cholesterol uptake is mediated through caveolae, cholesterol-rich plasma membrane surface microdomains, rich in caveolin-1 and SRB1 (3, 4). Western blotting of L-cell fibroblasts detected both caveolin-1 and SRB1 (data not shown). Indirect immunofluorescence and LSCM showed that caveolin-1 was localized in the cell surface (Fig. 7*A*) and in an intracellular pool (Fig. 7*B*), consistent with the literature showing caveolin-1 in plasma membrane caveolae, in Golgi/endoplasmic reticulum, and in a soluble complex (4). Indirect immunofluorescence identified two pools of SRB1, a surface associated pool (Fig. 7*C*) as well as a cytoplasmic pool (Fig. 7*D*), consistent with the literature (4). Pretreatment of L-cells for 30 min with filipin (2 and 10 μg/ml, respectively), which specifically inhibits HDL-mediated sterol uptake via caveolae but LDL receptor mediated uptake via clathrin coated pits (47, 48), increased the $t_{½}$ for HDL-mediated NBD-chol uptake 2.2- and 2.7-fold, respectively, from 102 ± 20 to 228 ± 17 and 272 ± 24 s (n = 3).

Molecular Basis for Targeting of Unesterified Sterol to Lipid Droplets—The molecular basis for unesterified sterol targeting to lipid droplets is not known. Very little is known whether the unesterified sterol in lipid droplets (44) is primarily present within the lipid phase or whether it is protein associated. The FRET data (see above), showing an intermolecular distance near 26 Å, suggested that unesterified sterols were present in the lipid phase, but did not exclude specific binding to protein in the lipid droplet. The best known lipid droplet protein, ADRP is localized to lipid droplets (43, 49), binds hydrophobic lipids such as NBD-stearic acid in 1:1 stoichiometry (50),[2] and increases fatty acid uptake (50). Therefore, the possibility that ADRP also binds unesterified sterol and is present in L-cell lipid droplets was examined.

The ability of ADRP to bind unesterified sterol was deter-

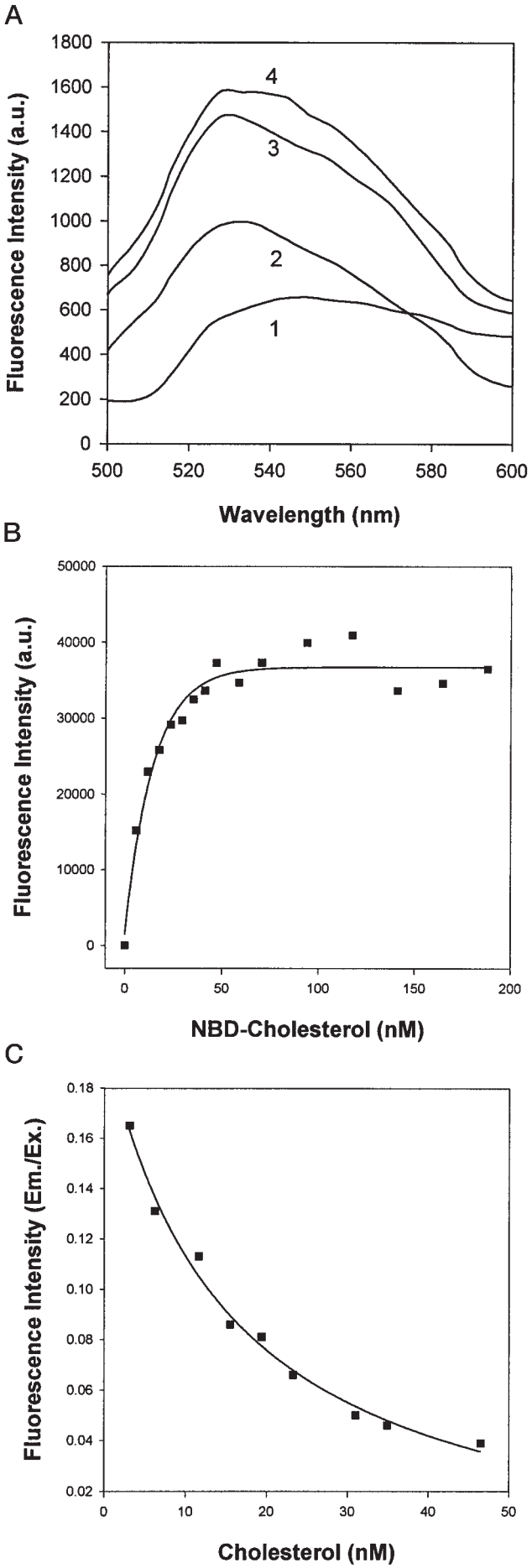

mined with mouse recombinant ADRP and a fluorescence sterol binding assay. The interaction of ADRP with NBD-chol was monitored as an increased fluorescence intensity and a blue shift in the NBD-chol emission maximum from 545 to 530 nm (Fig. 8*A*). ADRP exhibited saturation binding of NBD-chol (Fig. 8*B*). Analysis of the binding data showed that ADRP bound NBD-chol with high affinity, K_d = 2.0 nM, and 1:1 molecular stoichiometry. ADRP bound NBD-chol was effectively displaced by cholesterol, K_I = 13 nM (Fig. 8*C*), but not by ligands such as oleic acid and oleoyl-CoA (data not shown).

L-cells contained significant amounts of ADRP as revealed by Western blotting. L-cells expressed ADRP at a level intermediate with that of differentiated and undifferentiated 3T3 adipocytes (data not shown). As compared with the fibroblast-like, undifferentiated adipocytes, the expression of ADRP in L-cells was 4-fold higher. However, as compared with differentiated adipocytes, the expression of ADRP in L-cells was nearly 13-fold lower. Thus, ADRP expression in L-cells was within the range of cells accumulating lipid droplets.

Indirect immunofluorescence imaging revealed that ADRP was localized to lipid droplets in L-cells. Furthermore, ADRP colocalized with NBD-chol (Fig. 9) which in turn colocalized with Nile Red in lipid droplets of L-cells (Fig. 3). Single photon excitation LSCM with simultaneous acquisition of images for ADRP and NBD-chol showed a pattern of ADRP distribution (green) and NBD-chol distribution (red) that was very similar in L-cells (Fig. 9, *A* and *B*, respectively). Superposition of the simultaneously acquired images revealed a high degree of colocalization as shown by orange/yellow structures (Fig. 9*C*). The colocalization of ADRP with NBD-chol in lipid droplets in L-cells was quantitatively confirmed by the pixel fluorogram (Fig. 9*D*). In the pixel fluorogram most of the points were located away from the *x* and *y* axes. No colocalization would have been observed as two separate populations of points lying near the respective *x* and *y* axes. Finally, the *insets* in Fig. 9 show a magnification of a representative lipid droplet. A comparison of the NBD-chol staining of this lipid droplet (Fig. 9*A, inset*) with that of ADRP staining (Fig. 9*B, inset*) suggested that the diameter of the ADRP staining extended beyond that of the NBD-chol staining. To further validate this observation, the images of the lipid droplet in the insets of Fig. 9, *A* and *B*, were merged (Fig. 9*C, inset*). In the merged lipid droplet image (Fig. 9*C, inset*), the ADRP not colocalized with NBD-chol extended as a red ring or border beyond that of ADRP colocalized with NBD-chol shown as a yellow center in the lipid droplet. These data suggest that ADRP interacted both with the lipid phase as well as ADRP molecules extending beyond the lipid droplet surface. The relative proportion of NBD-chol associated with the lipid phase *versus* ADRP was evidenced by the preponderance of yellow pixels (ADRP associated NBD-chol) and only a small amount of green pixels (NBD-chol in the lipid phase not colocalized with ADRP).

Thus, ADRP was expressed in L-cells and localized to the surface of the lipid droplets. This location in conjunction with its high affinity for sterol (Fig. 8) suggested that the presence of

FIG. 8. **Sterol binding to ADRP.** *Panel A,* fluorescence emission spectra of NBD-chol without (*curve 1*) or with (*curves 2–4*) 70 nM ADRP in 25 mM phosphate buffer. NBD-chol was excited at 473 nm. From *bottom* to *top,* the NBD-chol concentrations were 25 nM (*curves 1* and *2*), 75 nM (*curve 3*) and 100 nM (*curve 4*). *Panel B,* saturation binding of NBD-chol (0 to 100 nM) to ADRP (11.1 nM). The intensities represent the maximal fluorescence intensity values are from a representative of four independent experiments. The data were fit to a simple, single binding site model as described under "Experimental Procedures." *Panel C,* displacement of ADRP bound NBD-chol by cholesterol. ADRP (70 nM) was preincubated with NBD-cholesterol (7 nM), followed by addition of displacing cholesterol (from 1.5 to 46.5 nM).

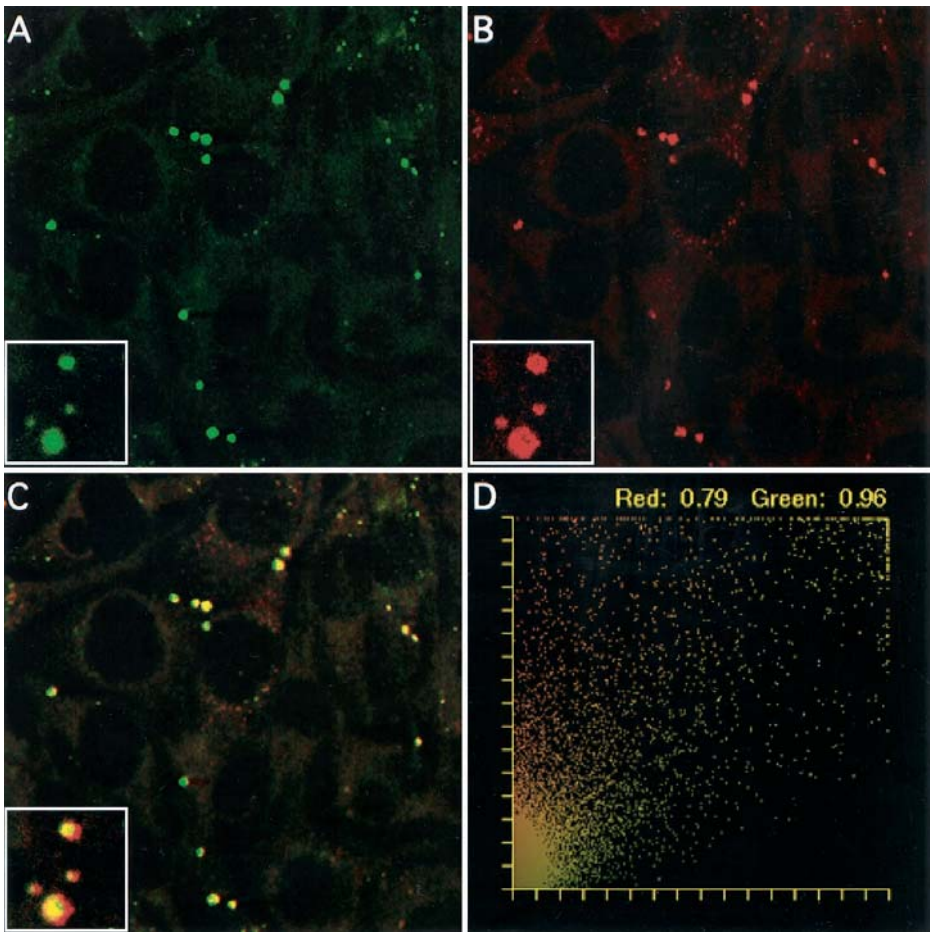

FIG. 9. **Indirect immunofluorescence of ADRP and NBD-Chol.** All procedures were as described under "Experimental Procedures." *A,* ADRP. *B,* NBD-chol. *C,* superimposed A and B to obtain a merged image. Colocalization is shown as *yellow-green*. *D,* pixel fluorogram showing high degree of colocalization of ADRP and NBD-chol. The *insets* in the figure, represent a typical lipid droplet in the dual labeled cells.

ADRP at the surface of the lipid droplet could account, at least in part, for the high degree of targeting of fluorescent sterols such as NBD-chol and DHE to lipid droplets in L-cells.

DISCUSSION

Although LDL receptor-mediated lipid metabolism has been characterized in depth over the past two decades, much less is known regarding the role of HDL in unesterified cholesterol dynamics, especially in living cells (for review, see Refs. 5, 51, and 52). In contrast to LDL receptor-mediated lipid uptake, this "alternate" pathway utilizes a completely different receptor (SRB1 receptor instead of LDL receptor), has a different apoprotein specificity (binds HDL as well as LDL and VLDL), is mediated through a different plasma membrane microdomain (caveolae instead of clathrin-coated pits), does not internalize (endocytose) whole lipoprotein particles, and takes up lipids in the order: cholesterol esters $\gg$ phosphatidylserine $>$ phosphatidylcholine = phosphatidylinositol $>$ sphingomyelin (53). Although HDL mediates cholesterol ester uptake in nonplacental steroidogenic tissues as well as cultured cells (for review, see Refs. 4 and 54) only recently was this visualized with fluorescent sterol ester (55). In contrast, while it is generally accepted that HDL mediates rapid efflux of cellular unesterified cholesterol, a process termed "reverse cholesterol transport," very little is actually known of HDLs role in uptake and intracellular targeting of unesterified cholesterol, especially in living cells (for review, see Refs. 5 and 54). The results of the present investigation provided several new insights on HDL-mediated uptake on unesterified sterol uptake.

First, comparison of the extent as well as $t_{1/2}$ of uptake for the fluorescent sterols, DHE and NBD-chol, to that of [^{3}H]cholesterol suggested that the two fluorescent sterols may selectively probe different uptake pathways. Although the uptake and half-time for maximal uptake of the fluorescent DHE resembled that of [^{3}H]cholesterol, NBD-chol uptake was $>$100-fold more rapid, but $>$100-fold less efficient. Recent data showed that NBD-chol uptake and flux through hamster intestine as well as NBD-chol uptake in Caco-2 cells is also markedly faster than that of radiolabeled cholesterol (24). Although it was suggested that these differences are due to lower affinity of NBD-chol for a cholesterol transporter or decreased solubility of NBD-chol, the present data suggested otherwise. NBD-chol has very high affinity (nM) for lipid-binding proteins such as ADRP (present data) and sterol carrier protein-2 (16, 56). Likewise, the critical micellar concentration of NBD-chol differs only 2-fold from that of DHE and cholesterol (27, 57). The two major receptor-mediated sterol transport pathways differ markedly in speed: slow (15–45 min) LDL receptor-mediated (endocytic) uptake (for review, see Ref. 52); fast (1 min) HDL receptor-mediated efflux of cholesterol (for review, see Ref. 4). These data, taken together with the lipoprotein (HDL *versus* LDL and VLDL) specificity of NBD-chol uptake shown herein and earlier for esterified cholesterol (for review, see Refs. 5, 53–55, and 58) as well as the effects of filipin on NBD-chol uptake shown herein and on cholesterol ester uptake elsewhere (for review, see Refs. 47, 48, and 55) were consistent with the uptake of the two fluorescent, unesterified sterols being mediated, at least in part, by different mechanism(s).

Second, once internalized the DHE and NBD-chol appear to follow similar pathways to be esterified as compared with [^{3}H]cholesterol. At equimolar concentrations these sterols differed less than $<$2-fold in esterification. L-cell esterification of DHE confirms an earlier study (2) while that of NBD-chol clari-

fies a controversy in the literature (see Introduction). NBD-chol is esterified *in vivo* by hamster intestine and Caco-2 cells, derived from intestine, as well as *in vitro* by intestinal microsomes (24). In contrast, rat liver microsomes did not esterify NBD-chol (25). The different observations may be due to differences in the substrate specificities of the two known acyl-CoA cholesterol acyltransferases (1 or 2). Acyl-CoA:cholesterol *O*-acyltransferase 1 is absent from intestinal cells while liver contains both acyl-CoA:cholesterol *O*-acyltransferase 1 and 2 (59).

Third, once internalized the fluorescent sterols rapidly target to lipid droplets. LSCM and MLSM imaging, colocalization with Nile Red, and FRET all indicated specific targeting of the HDL-mediated unesterified sterol uptake to lipid droplets. This process was specific for the HDL-mediated uptake of unesterified (shown herein) and esterified sterols, but not DiI (55). The speed (<30 s) of HDL-mediated NBD-chol targeting to lipid droplets was much faster than that of HDL-mediated uptake of BODIPY-cholesterol ester, 5 min (55). However, this very rapid (<30 s) intracellular transfer of unesterified NBD-chol was similar to that of endogenously synthesized cholesterol from the endoplasmic reticulum to the cell surface, 1 min (for review, see Ref. 4), and implied a nonvesicular pathway(s). Several candidate intracellular cholesterol-binding proteins (sterol carrier protein-2, caveolin-1, steroidogenic acute regulatory protein, etc.) for such a nonvesicular mechanism have been proposed (for review, see Refs. 4 and 16).

Fourth, the specific targeting of unesterified cholesterol to lipid droplets may be mediated, at least in part by ADRP, a lipid droplet specific protein (49). ADRP in L-cells was localized on the surface of lipid droplets as in other cell types (43). More important, indirect immunofluorescence revealed that the ADRP was highly colocalized with NBD-chol in the lipid droplet. Finally, ADRP specifically bound NBD-chol with high affinity (K_d = 2 nM), suggesting that this colocalization was due at least in part to direct binding of NBD-chol ADRP. This affinity was in the same range of that of other known sterol-binding proteins, *e.g.* sterol carrier protein-2 with K_d = 6–11 nM (16, 57). Since ADRP has been shown to also bind fatty acid (50),[2] this would indicate that ADRP can bind several types of lipid substrates, similar to sterol carrier protein-2 (30, 56, 57, 60–62).

In summary, the data presented herein were consistent with DHE and NBD-chol uptake preferentially taking place by different pathways, *e.g.* LDL receptor endocytic *versus* HDL receptor molecular transfer via caveolae. Furthermore, both DHE and NBD-chol demonstrated specific targeting of unesterified sterol to lipid droplets, a process that was very rapid and potentially mediated by ADRP, a lipid-binding protein specific to droplets. Thus, these data provided basic new observations contributing to our understanding of HDL receptor-mediated uptake of unesterified cholesterol, its intracellular dynamics, and its targeting to lipid droplets, an organelle about which very little is known (43, 45, 49).

REFERENCES

1. Schroeder, F., Woodford, J. K., Kavecansky, J., Wood, W. G., and Joiner, C. (1995) *Mol. Membr. Biol.* **12,** 113–119
2. Schroeder, F., Frolov, A. A., Murphy, E. J., Atshaves, B. P., Jefferson, J. R., Pu, L., Wood, W. G., Foxworth, W. B., and Kier, A. B. (1996) *Proc. Soc. Exp. Biol. Med.* **213,** 150–177
3. Fielding, C. J., and Fielding, P. E. (1997) *J. Lipid. Res.* **38,** 1503–1521
4. Smart, E. J., and van der Westhuyzen, D. R. (1998) in *Intracellular Cholesterol Trafficking* (Chang, T. Y., and Freeman, D. A., eds) pp. 253–272, Kluwer Academic Publishers, Boston
5. Stangl, H., Cao, G., Wyne, K. L., and Hobbs, H. H. (1998) *J. Biol. Chem.* **273,** 31002–31008
6. Schroeder, F. (1984) *Prog. Lipid Res.* **23,** 97–113
7. Schroeder, F. (1985) in *Subcellular Biochemistry* (Roodyn, D. B., ed) pp. 51–101, Plenum Press, New York
8. Schroeder, F., and Nemecz, G. (1990) in *Advances in Cholesterol Research* (Esfahani, M., and Swaney, J., eds) pp. 47–87, Telford Press, Caldwell, NJ
9. Nemecz, G., Fontaine, R. N., and Schroeder, F. (1988) *Biochim. Biophys. Acta* **943,** 511–521
10. Schroeder, F., Goh, E. H., and Heimberg, M. (1979) *FEBS Lett.* **97,** 233–236
11. Schroeder, F., Goh, E. H., and Heimberg, M. (1979) *J. Biol. Chem.* **254,** 2456–2463
12. Hale, J. E., and Schroeder, F. (1982) *Eur. J. Biochem.* **122,** 649–661
13. Schroeder, F., Nemecz, G., Wood, W. G., Joiner, C., Morrot, G., Ayraut-Jarrier, M., and Devaux, P. F. (1991) *Biochim. Biophys. Acta* **1066,** 183–192
14. Smutzer, G., Crawford, B. F., and Yeagle, P. L. (1986) *Biochim. Biophys. Acta* **862,** 361–371
15. Schroeder, F., Barenholz, Y., Gratton, E., and Thompson, T. E. (1987) *Biochemistry* **26,** 2441–2448
16. Schroeder, F., Frolov, A., Schoer, J., Gallegos, A., Atshaves, B. P., Stolowich, N. J., Scott, A. I., and Kier, A. B. (1998) in *Intracellular Cholesterol Trafficking* (Chang, T. Y., and Freeman, D. A., eds) pp. 213–234, Kluwer Academic Publishers, Boston
17. Wood, W. G., Schroeder, F., Avdulov, N. A., Chochina, S. V., and Igbavboa, U. (1999) *Lipids* **34,** 225–234
18. Frolov, A., Woodford, J. K., Murphy, E. J., Billheimer, J. T., and Schroeder, F. (1996) *J. Biol. Chem.* **271,** 16075–16083
19. Frolov, A. A., Woodford, J. K., Murphy, E. J., Billheimer, J. T., and Schroeder, F. (1996) *J. Lipid. Res.* **37,** 1862–1874
20. Smith, R. J. M., and Green, C. (1974) *Biochem. J.* **137,** 413–415
21. Bergeron, R. J., and Scott, J. (1982) *Anal. Chem.* **119,** 128–134
22. Bergeron, R. J., and Scott, J. (1982) *J. Lipid Res.* **23,** 391–404
23. Mukherjee, S., Zha, X., Tabas, I., and Maxfield, F. R. (1998) *Biophys. J.* **75,** 1915–1925
24. Sparrow, C. P., Patel, S., Baffic, J., Chao, Y.-S., Hernandez, M., Lam, M.-H., Montenegro, J., Wright, S. D., and Detmers, P. A. (1999) *J. Lipid Res.* **40,** 1747–1757
25. Billheimer, J. T., and Gillies, P. J. (1990) in *Advances in Cholesterol Research* (Esfahani, M., and Swaney, J. B., eds) pp. 7–45, The Telford Press, Caldwell, NJ
26. Schroeder, F., Perlmutter, J. F., Glaser, M., and Vagelos, P. R. (1976) *J. Biol. Chem.* **251,** 6739–6746
27. Fischer, R. T., Cowlen, M. S., Dempsey, M. E., and Schroeder, F. (1985) *Biochemistry* **24,** 3322–3331
28. Schroeder, F., Perlmutter, J. F., Glaser, M., and Vagelos, P. R. (1976) *J. Biol. Chem.* **251,** 5015–5026
29. Laemmli, U. K. (1970) *Nature* **227,** 680–685
30. Schroeder, F., Myers-Payne, S. C., Billheimer, J. T., and Wood, W. G. (1995) *Biochemistry* **34,** 11919–11927
31. Masters, B. P., and So, P. T. C. (1997) *Biophys. J.* **72,** 2405–2412
32. So, P. T. C., French, T., Yu, W. M., Berland, K. M., Dong, C. Y., and Gratton, E. (1996) in *Fluorescence Imaging Spectroscopy and Microscopy* (Wang, X. G., and Herman, B., eds) p. 351, John Wiley & Sons, Inc., Boston
33. Forster, T. (1967) in *Comprehensive Biochemistry* (Florkin, M., and Statz, E. H., eds) pp. 61–77, Elsevier, New York
34. Loura, L. M. S., and Prieto, M. (1997) *Biophys. J.* **72,** 2226–2236
35. Hara, A., and Radin, N. S. (1978) *Anal. Biochem.* **90,** 420–426
36. Bradford, M. M. (1976) *Anal. Biochemistry* **72,** 248–254
37. Murphy, E. J. (1998) *Am. J. Physiol.* **275,** G237–G243
38. Murphy, E. J., and Schroeder, F. (1997) *Biochim. Biophys. Acta* **1345,** 283–292
39. Moncecchi, D. M., Murphy, E. J., Prows, D. R., and Schroeder, F. (1996) *Biochim. Biophys. Acta* **1302,** 110–116
40. Denk, W., Strickler, J. H., and Webb, W. W. (1990) *Science* **248,** 73–76
41. Maiti, S., Shear, J. B., Williams, R. M., Zipfel, W. R., and Webb, W. W. (1997) *Science* **275,** 530–532
42. Fowler, S. D., and Greenspan, P. (1985) *J. Histochem. Cytochem.* **33,** 833–836
43. Brasaemle, D. L., Barber, T., Wolins, N., Serrero, G., Blanchette-Mackie, E. J., and Londos, C. (1997) *J. Lipid Res.* **38,** 2249–2263
44. Chanderbhan, R., Noland, B. J., Scallen, T. J., and Vahouny, G. V. (1982) *J. Biol. Chem.* **257,** 8928–8934
45. Londos, C., Brasaemle, D. L., Schultz, C. J., Segrest, J., and Kimmel, A. R. (1999) *Cell Dev. Biol.* **10,** 51–58
46. Murphy, E. J., and Schroeder, F. (1997) *Biochim. Biophys. Acta* **1345,** 283–292
47. Schnitzer, J. E., Allard, J., and Oh, P. (1995) *Am. J. Physiol.* **268,** H48–H55
48. Schnitzer, J. E., Liu, J., and Oh, P. (1995) *J. Biol. Chem.* **270,** 14399–14404
49. Jiang, H. P., and Serrero, G. (1992) *Proc. Natl. Acad. Sci. U. S. A.* **89,** 7856–7860
50. Gao, J., and Serrero, G. (1999) *J. Biol. Chem.* **274,** 16825–16830
51. Krieger, M. (1998) *Proc. Natl. Acad. Sci. U. S. A.* **95,** 4077–4080
52. Fielding, C. J., Bist, A., and Fielding, P. E. (1998) in *Intracellular Cholesterol Trafficking* (Chang, T. Y., and Freeman, D. A., eds) pp. 273–288, Kluwer Academic Publishers, Boston
53. Rodrigueza, W. V., Thuanhnai, S. T., Temel, R. E., Lund-Katz, S., Phillips, M. C., and Williams, D. L. (1999) *J. Biol. Chem.* **274,** 20344–20350
54. Acton, S., Rigotti, A., Landschulz, K. T., Xu, S., Hobbs, H. H., and Krieger, M. (1996) *Science* **271,** 518–520
55. Reaven, E., Tsai, L., and Azhar, S. (1996) *J. Biol. Chem.* **271,** 16208–16217
56. Stolowich, N., Frolov, A., Petrescu, A., Scott, A. I., Billheimer, J. T., and Schroeder, F. (1999) *J. Biol. Chem.* **274,** 35425–35433
57. Avdulov, N. A., Chochina, S. V., Igbavboa, U., Warden, C. H., Schroeder, F., and Wood, W. G. (1999) *Biochim. Biophys. Acta* **1437,** 37–45
58. Acton, S. L., Scherer, P. E., Lodish, H. F., and Krieger, M. (1994) *J. Biol. Chem.* **269,** 21003–21009
59. Yu, C., Chen, J., Lin, S., Liu, J., Chang, C. C. Y., and Chang, T.-Y. (1999) *J. Biol. Chem.* **274,** 36139–36145
60. Frolov, A., Cho, T. H., Billheimer, J. T., and Schroeder, F. (1996) *J. Biol. Chem.* **271,** 31878–31884
61. Colles, S. M., Woodford, J. K., Moncecchi, D., Myers-Payne, S. C., McLean, L. R., Billheimer, J. T., and Schroeder, F. (1995) *Lipids* **30,** 795–804
62. Stolowich, N. J., Frolov, A., Atshaves, B. P., Murphy, E., Jolly, C. A., Billheimer, J. T., Scott, A. I., and Schroeder, F. (1997) *Biochemistry* **36,** 1719–1729